

Manipulation and Assessment of Human Red Blood Cells with Tunable “Tug-of-War” Optical Tweezers

Yi Liang^{1,2,*}, Guo Liang^{2,3}, Yinxiao Xiang², Josh Lamstein², Rekha Gautam^{2,4},
Anna Bezryadina^{2,5} and Zhigang Chen^{2,6,†}

¹*Guangxi Key Lab for Relativistic Astrophysics, Center on Nanoenergy Research, School of Physical Science and Technology, Guangxi University, Nanning, Guangxi 530004, China*


²*Department of Physics and Astronomy, San Francisco State University, San Francisco, California 94132, USA*

³*School of Physics and Electrical Information, Shangqiu Normal University, Shangqiu 476000, China*

⁴*Department of Biomedical Engineering, Vanderbilt University, Nashville, Tennessee 37240, USA*

⁵*Department of Physics and Astronomy, California State University Northridge, Northridge, California 91330, USA*

⁶*MOE Key Lab of Weak-Light Nonlinear Photonics, TEDA Applied Physics Institute and School of Physics, Nankai University, Tianjin 300457, China*

 (Received 17 October 2019; revised manuscript received 24 November 2019; published 27 December 2019)

Understanding the biomechanical properties of red blood cells (RBCs) is crucial for many pathological analyses and diagnoses of human diseases. Here, we construct the so-called “tug-of-war” (TOW) optical tweezers, consisting of a pair of elongated diverging beams, to study the deformability of human RBCs. Such an optical tweezers system gives rise to object-adapted optical potentials that can stably trap, squeeze, and stretch single RBCs under different osmotic conditions without tethering or mechanical movement. Even at low trapping power, the TOW tweezers can exert a force of 18 pN, which is at least two times stronger than that of dual-trap optical tweezers based on conventional Gaussian beams, leading to more than 15% deformation of the cell shape. From a direct comparison of the trapping forces and shear modulus of the RBCs under different osmotic conditions, we find that the cell deformability follows a trend: hypotonic > isotonic > hypertonic. This work exemplifies another photonic tool with advanced beam-shaping techniques for biomechanical studies of living cells that is promising for applications such as distinguishing healthy and diseased cells and intracellular delivery.

DOI: [10.1103/PhysRevApplied.12.064060](https://doi.org/10.1103/PhysRevApplied.12.064060)

I. INTRODUCTION

Erythrocytes or red blood cells (RBCs), which are integral to human body metabolism, transport oxygen and carbon dioxide between body tissues by deforming to squeeze through narrow capillaries. Indeed, RBC deformability and associated biomechanical properties play an important role in many pathological analyses and diagnoses of human diseases, such as malaria, sickle cell disease, diabetes mellitus, and thalassemia [1–5]. Many factors can affect the deformability of RBCs, such as hemoglobin concentration, osmolarity, and cell age [2,3,5]. Any change of these properties may affect the function of the RBCs, causing blood-related diseases. RBC deformability may be used as a biomarker to determine the pathophysiological states of the RBCs [2–6] and to gauge the effects of drug treatment on RBC-mediated diseases [7].

There are many established techniques to measure the mechanical deformability of RBCs, such as atomic force microscopy, magnetic twisting cytometry, micropipette aspiration, shear-flow methods, and optical trapping techniques [2–4,8–10]. Nowadays, optical trapping techniques are routinely used for stretching RBCs to determine their deformability because optical trapping techniques provide a quick noncontact force measurement tool in a liquid medium with piconewton- (pN) resolution accuracy.

Optical trapping methods can be classified mainly into two categories. The first category is direct manipulation of cells, which includes dual-trap optical tweezers [6,7,11,12], optical stretchers with two counterpropagating laser beams [13–15], specially shaped single-beam optical tweezers [16–18], and single-beam optical traps in combination with fluid flow or electric fields [19–23]. The second category can be considered as indirect manipulation of cells, which typically relies on tethering cells to a well-defined bead or its other variations (such as gripper formation with several beads to manipulate the target cell) [24–35]. As is usually the case, each technique has its

*liangyi@gxu.edu.cn

†zhigang@sfsu.edu

own limitations in characterizing cell deformation. Direct manipulation is relatively simple and fast, but it could cause photodamage to RBCs from prolonged exposure or high trapping powers [10,24,25]. It has been shown that damage induced in RBCs could lead to large enhancement of cell rigidity (and thus, reduced RBC deformability) after merely minutes of laser exposure [25]. The indirect manipulation technique involves a more complicated process of attaching beads to a single RBC from opposite sides [24]

Recently, the design of optical tweezers based on two “tug-of-war” (TOW) optical beams was proposed and demonstrated [36,37]. In the appropriate context, the design leads to more efficient cell stretching compared with that of Gaussian-beam-based dual optical tweezers. The TOW tweezers consist of two transverse elongated diverging beams, with a tunable separation angle and a steep intensity gradient that increases radially inward [see Fig. 1(b) and Video 1 within the Supplemental Material [38]]. It is demonstrated that, compared with conventional dual-trap optical tweezers, TOW optical tweezers can be implemented as a direct manipulation method for cell trapping and stretching with much less photodamage. Photodamage is reduced because the beams are elongated in the observation plane and diverge in the propagation direction. In particular, such TOW optical tweezers can generate large lateral pulling forces on a trapped object and hold it stably in an observing plane [36]. Furthermore, here, we report that TOW optical tweezers can also be used as a direct squeezer of cells, which cannot be done with two conventional Gaussian beams without attaching beads. The ability to squeeze cells with the TOW tweezers may be useful for studying multiple cell biomechanical properties with a standard holographic optical trapping system.

Here, we employ TOW optical tweezers to trap, squeeze, and stretch single RBCs under different osmotic conditions, without any tethering or mechanical movement,

thereby quantitatively characterizing the deformability of RBCs. With a viscous drag method, we measure directly the trapping forces that act on RBCs under different conditions and estimate that the force from just one side of the TOW tweezers can be over 18 pN, with approximately 20 mW laser power, which is more than double that with the force from conventional optical tweezers (Gaussian trap) under the same conditions. Meanwhile, the spacing between the two traps in the TOW tweezers can be increased easily from 0 to over $9\ \mu\text{m}$ without multiple independent user controls for each side of the beam, resulting in over 15% shape deformation of cells after squeezing or stretching. The shear modulus of the RBCs under different osmotic conditions is also calculated, and the largest value of $3.36 \pm 0.95\ \text{pN}\ \mu\text{m}^{-1}$ is found for the hypertonic condition. Moreover, by use of the TOW tweezers, we illustrate the transformation of a RBC between a squeezed state and a stretched state. Our work suggests that the TOW tweezers may be applied to biomedical or microengineering in the study of the biomechanical properties of living cells or intracellular delivery [39–41].

II. MATERIALS AND METHODS

Fresh blood samples from healthy donors are collected in ethylenediamine tetra-acetic acid (EDTA) tubes and centrifuged three times at 3500 rpm for 5 min. Each time, the upper layer of the RBC suspension is removed, and the remaining RBCs are washed and centrifuged in RPMI 1640 (Roswell Park Memorial Institute 1640 medium, R8758, Sigma-Aldrich). First, three different buffers are prepared by varying only the NaCl concentration ($8.182\ \text{mg}\ \text{ml}^{-1}$ for isotonic, $4.0\ \text{mg}\ \text{ml}^{-1}$ for hypotonic, and $14.0\ \text{mg}\ \text{ml}^{-1}$ for hypertonic conditions), while keeping the concentration of the other three salts constant (KCl, $0.201\ \text{mg}\ \text{ml}^{-1}$; Na_2HPO_4 , $1.434\ \text{mg}\ \text{ml}^{-1}$;

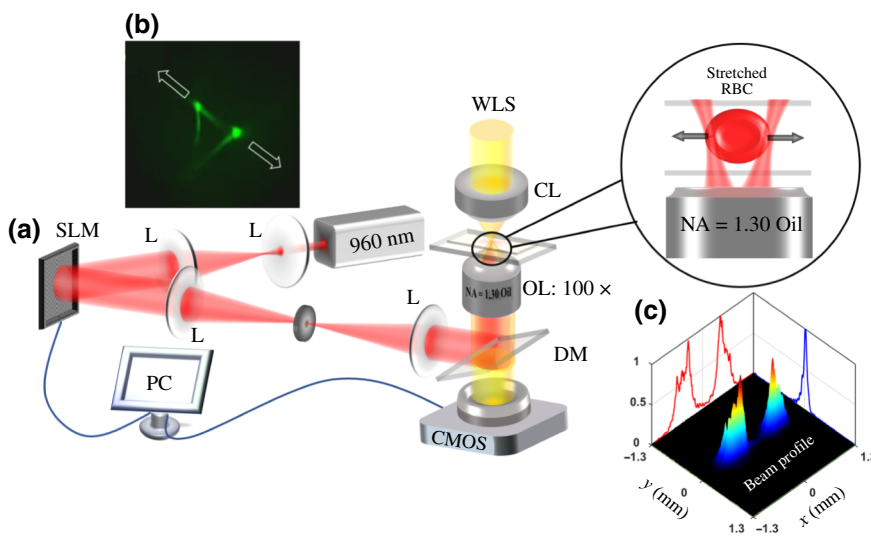


FIG. 1. Manipulating and accessing human RBCs with tunable TOW optical tweezers. (a) Schematic of the TOW optical tweezers setup for manipulation and assessment of RBCs. L, lens; SLM, spatial light modulator; DM, dichroic mirror; OL, 100 \times objective lens; CL, condenser lens; WLS, white-light source; CMOS, camera; PC, computer. The inset illustrates a stretched RBC under the action of the TOW tweezers. (b) Three-dimensional image of the TOW beam obtained in experiments, where the arrows indicate force directions in the trapping plane. (c) Normalized intensity distribution of the TOW beam, showing a sharp intensity gradient on one side. Red and blue lines describe the beam profiles along the x and y directions, respectively.

and KH_2PO_4 , 0.245 mg ml^{-1}). Then, $2 \mu\text{l}$ washed RBCs are diluted in 2.5 ml isotonic, hypotonic, and hypertonic buffers to prepare RBC samples of different osmotic conditions. For each RBC solution, about $50 \mu\text{l}$ is injected into a sample chamber, consisting of a microscope slide and a coverslip with about $100 \mu\text{m}$ spacing. Notably, a small amount (approximately 1 mg ml^{-1}) of bovine serum albumin (BSA) is also added to the RBC solution to prevent the cells from sticking to the sample chamber walls. Finally, the prepared RBC chamber is placed on the stage of the TOW optical tweezers system for experimental measurements. As expected, we observe that the “normal” RBCs exhibit a biconcave disk shape in the isotonic phosphate-buffered saline (PBS), while the “swollen” RBCs have a spherical shape in the hypotonic buffer and the “shrunken” RBCs present an irregular spiky shape in the hypertonic buffer [Figs. 2(b)–2(d)]; these shape changes are largely due to the uptake or release of water from the cells under varied osmotic pressure [42–45].

The TOW optical tweezers can be generated by creating two diverging elongated beams [Fig. 1(b)], with a SLM that acts as a combination of a cylindrical lens and a prism [36]. For a real-time flexible manipulation of RBCs without mechanical movement, the holographic optical tweezers approach is taken, as schematically shown in Fig. 1(a). A 960 nm linearly polarized laser beam is expanded and directed into the SLM programmed with a desired hologram for generating the TOW trapping beam, which is then propagated through a $4f$ imaging system and directed into a $100\times$ oil-immersion objective with a high numerical aperture ($\text{NA} = 1.30$). For examining and recording the process of RBC stretching, a white-light

source passing through a condenser lens illuminates the sample. The spacing between the two arms of the TOW tweezers is controlled by changing parameters (such as the prism apex angle and the focal length of the cylindrical lens) of the designed hologram. The laser power is also varied from 0 to 40 mW, as measured before illuminating the sample [after the objective lens shown in Fig. 1(a)]. Figure 1(c) displays the intensity profile of the TOW beam before being launched into the objective lens, showing two stripelike beams with asymmetric intensity distribution along the stretching x direction [36]. For systematic analysis and fair comparison, the experiments are performed with at least eight different cell samples using the same preparation at each osmotic condition.

III. RESULTS AND DISCUSSION

Before manipulating and accessing RBC deformability with the TOW tweezers, force calibrations are performed for the RBCs for each osmotic condition by utilizing the viscous-drag-force calibration method [18,26,35]. For this purpose, a single RBC is trapped by only one arm of the TOW optical tweezers, as shown in Fig. 2(a), and then the chamber on the piezostage is driven away from the optical axis of the system at a constant velocity until the cell escapes. (Notably, the other TOW arm is still there, and we block it with a spatial filter, since the two arms are well separated.) In equilibrium, the trapped RBC experiences zero net force, as the velocity-dependent viscous drag force and the pulling optical trapping force cancel each other out. Increasing the velocity further, and thus, increasing the drag force, would eventually overcome the

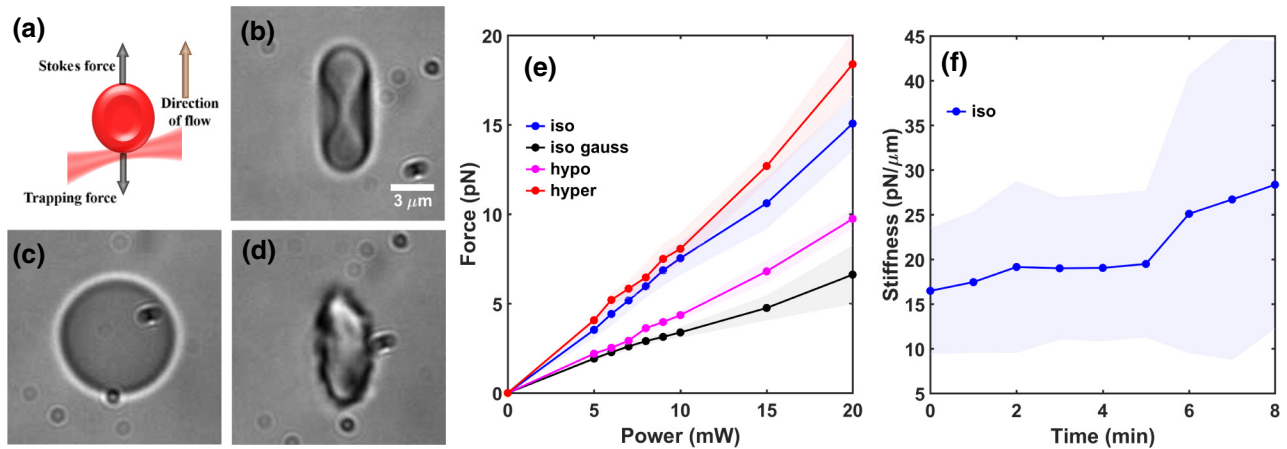


FIG. 2. Force calibrations of the TOW tweezers on the RBCs. (a) Schematic illustration of the drag method for measuring the force from one arm of the TOW tweezers. Single RBC images recorded in (b) isotonic, (c) hypotonic, and (d) hypertonic buffers. (e) Measurement of the maximal optical trapping forces generated by one arm of the TOW tweezers as a function of incident laser power at the focal plane under different conditions. The black line depicts the results measured with a conventional Gaussian-beam trap in isotonic solution for direct comparison. (f) Measured stiffness change as a function of exposure time for a RBC trapped by the TOW tweezer with 20 mW power in isotonic solution. The measurement error ranges are indicated by the shaded regions surrounding the respective curves.

optical trapping force and lead to the cell escaping from the tweezers, thereby determining the maximum trap force. Videos 2–4 within the Supplemental Material [38] show the dynamic process of a cell escaping from the trap in isotonic [Fig. 2(b)], hypotonic [Fig. 2(c)], and hypertonic [Fig. 2(d)] solutions. Approximating the RBC as an ellipsoid, one can estimate the maximal trapping force, F_{trap} , from one arm of the TOW tweezers, since it must equal the escaping viscous drag force, F_{drag} , which can be calculated from a modified Stokes equation [18,26,35,46]:

$$F_{\text{trap}} = F_{\text{drag}} = 6\pi\eta v \left(\frac{1}{3}r_1/f_1 + \frac{2}{3}r_2/f_2 \right),$$

$$f_n = \left[1 - \frac{9}{16} \left(\frac{r_n}{h} \right) + \frac{1}{8} \left(\frac{r_n}{h} \right)^3 - \frac{45}{256} \left(\frac{r_n}{h} \right)^4 - \frac{1}{16} \left(\frac{r_n}{h} \right)^5 \right], n = 1, 2, \quad (1)$$

where η is the viscosity of the solution, v is the critical flow velocity of the fluid leading to escape of the cell from the trap, r_1 is the radius of a sphere with the same cross-section area of a RBC, r_2 is the radius of a sphere with the same surface area as that of the RBC stretched by the flow, f_n is a drag correction factor due to the chamber surface, and h is the distance from the center of the trapped RBC to the surface [18,26]. According to our experiment, the parameters are taken as $h \approx 50 \mu\text{m}$ and $\eta = 0.001 \text{ Pa s}$, due to the low concentration of RBCs in the solutions.

The measured average forces calculated from experimental data recorded under different solutions are presented in Fig. 2(e). All forces are proportional to the laser power, which is consistent with previous work [26–28,46]. Interestingly, our findings show that, for the same power level, the force experienced by a RBC is largest in the hypertonic solution and smallest in the hypotonic solution. At all power levels, the force from one TOW trap is always larger than that of the force from a Gaussian trap. Taking the isotonic solution as an example for comparison, the trapping force generated by one arm of the TOW tweezers reaches 15 pN, which is about two times stronger than that created by its Gaussian counterpart (6.6 pN) at the same beam power (20 mW). In other words, we can achieve the same force, but with lower power, as that of a Gaussian trap. Due to the special shaping of the TOW beam, the photon density on the surface of the cells is also significantly reduced, and thus, further increases the photodamage threshold. To demonstrate this, we also investigate the stiffness of the isotonic RBCs, as an example, trapped by the TOW tweezers at 20 mW power during 8 min [Fig. 2(f)]. Clearly, the TOW induces a stiffness increase that is only appreciable after 5 min of light exposure. However, compared with previous work [25], this change of

stiffness with time is much less dramatic, which indicates reduced photodamage with the TOW tweezers.

With approximately 20 mW of power from one arm of the TOW tweezers illuminating the sample in the hypertonic and hypotonic solutions, the maximum force obtained is 18 and 10 pN, respectively. Theoretically, such a trend in the trapping force at different osmotic pressures can also be explained in terms of changes to the cell shape and the hemoglobin concentration of the RBCs in different buffer solutions. The refractive indices at the three studied osmotic conditions are different: $n \sim 1.38$ for hypotonic, $n \sim 1.42$ for isotonic, and $n \sim 1.44$ for hypertonic solutions [47,48], i.e., the effective refractive indices, n , of the RBCs follow the trend $n_{\text{hypotonic}} < n_{\text{isotonic}} < n_{\text{hypertonic}}$. Because the average size of the RBCs ($\sim 8 \mu\text{m}$) is almost an order of magnitude larger than that of the laser wavelength ($0.96 \mu\text{m}$) used, we can use the geometric ray optics approximation. The gradient force is given by $F_{\text{grad}} \sim Qn_m P/c$, where Q is the trapping efficiency related to $n = n_p/n_m$; P and c are the power and speed of light, respectively. As such, the trapping force is related to the effective refractive index difference between the particle (n_p) and the ambient medium (n_m) [46] and is expected to follow the same trend as that of the refractive indices. Notably, the RBCs are trapped by only one arm of the TOW tweezers for these calibration experiments, as opposed to the two-arm stretching experiments discussed below.

To examine the potential of the TOW tweezers, we study the effect of applying both arms to the RBCs trapped under different osmotic conditions. A RBC can be trapped and rotated stably and reliably in a given observation plane (see Video 5 within the Supplemental Material [38]). More importantly, the RBCs can be efficiently squeezed and stretched to assess deformation, as illustrated in Fig. 3, where Figs. 3(a)–3(c) show the results obtained under different osmotic conditions. When the spacing between the two arms is smaller than that of the cell diameter, the TOW tweezers squeeze (rather than stretch) the RBCs [Figs. 3(a2)–3(c2)]. When the spacing is increased above a certain value, the RBCs are stretched and their vertical axial diameter increases [Figs. 3(a3)–3(c3)]. For different osmotic conditions, the maximum RBC deformation is reached at different TOW spacing [Figs. 3(a4)–3(c4)] (the maximum size change is determined and limited by the maximum spacing of the TOW). When the spacing increases beyond the limit, the tweezers cannot keep a RBC stable in both traps. Consequently, the RBC tends to escape from one arm of the TOW tweezers and be trapped only by the other arm (see Videos 6–8 within the Supplemental Material [38]).

To quantitatively analyze our experimental results, we perform a detailed comparison of the morphological transformation of the RBC under different osmotic conditions. We plot the axial diameter change as a function of the spacing between two arms of the TOW tweezers, as shown

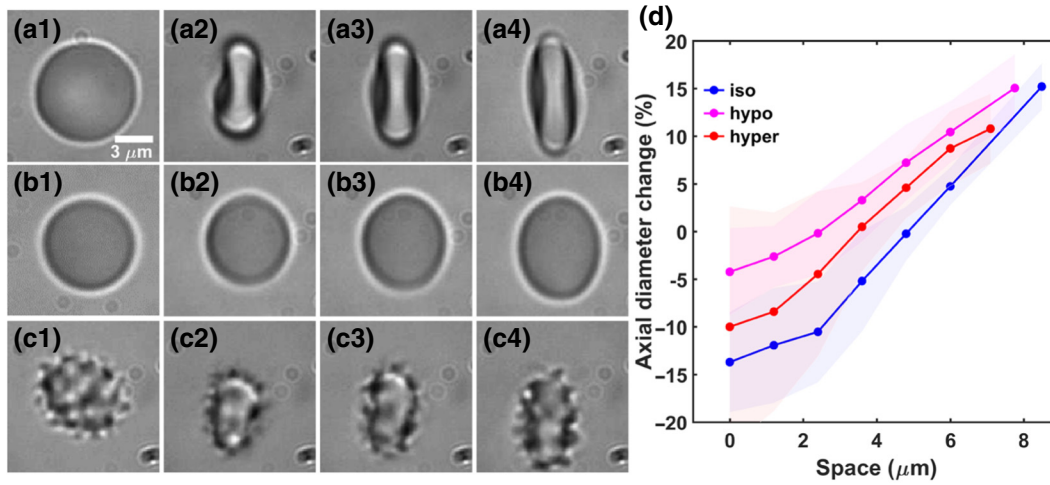


FIG. 3. Spacing dependences of deformation of RBCs via TOW tweezers. (a)–(c) Results of RBC stretching in different buffers: (a) isotonic, (b) hypotonic, and (c) hypertonic. The spacing between two arms of the TOW tweezers is varied, while the laser power at the focal plane is fixed at 40 mW. The first column shows the images of a RBC in different buffers without the trapping beam. The second and third columns illustrate the RBC shape change when the spacing is 2.4 and 4.8 μm , respectively. The fourth column shows the cell deformation at the largest spacing of the TOW tweezers arms, which is 9.8 μm (a4), 8.8 μm (b4), and 8.0 μm (c4). (d) Measured percentage change of the axial diameter of the trapped RBC under different conditions as a function of the spacing between the two arms of the TOW beam.

in Fig. 3(d). One can clearly see the axial diameter change under different osmotic conditions. Because the shape of the RBCs changes under different osmotic conditions, the TOW spacing needed to transform a RBC from a squeezed state to a stretched state varies accordingly: 2.5 μm for the hypotonic solution, 4.9 μm for the isotonic solution, and 3.5 μm for the hypertonic solution. Moreover, it can be seen from Fig. 3(d) that the hypotonic RBCs tend to exhibit the largest axial diameter change, if the same laser power and the same spacing are used. At the largest spacing achievable with the TOW beam, which means the RBCs are still stably trapped by both arms of the TOW tweezers, both hypotonic and isotonic RBCs reach over 15% change in cell size with a power of 40 mW. However, this does not mean that these two kinds of RBCs exhibit the same deformability because, under different osmotic conditions, the RBCs experience different maximal optical force strengths at the same laser power, as shown in Fig. 2(e): about 9.7 pN for the hypotonic, 15.1 pN for the isotonic, and 18.4 pN for the hypertonic. We emphasize that, although a similar relative change in cell size has been demonstrated before with dual-trap optical tweezers, the required laser power is typically much higher (about 90 mW or more) [7,26]. In addition, due to the special beam shaping, the TOW tweezers reduce the photodamage to the cells, relative to that of their Gaussian-trap counterparts.

For a more effective and reliable comparison of the deformability of RBCs under different osmotic conditions, we compare directly the stretched axial diameter of the RBC as a function of the applied force strength,

as illustrated in Fig. 4(a). Similar approaches have been applied in previous works [26–31]. Hypotonic RBCs are the easiest to stretch, while hypertonic RBCs are the most difficult to stretch; this is consistent with previous results [29]. The hypotonic RBCs deform almost linearly with increasing applied force strength, while the hypertonic and isotonic RBCs exhibit a nonlinear trend of deformation under strong stretching forces. When the deformation is small for a reasonable range of trap spacing, the RBCs under all three conditions exhibit linear deformation. The difference of cell deformation in response to stretching forces comes from different cell elasticity, since the hypotonic RBCs are the most malleable, while the hypertonic cells are the most rigid. Different trends of deformation with respect to the spacing between two sides of the TOW beam under different osmotic conditions may also be seen in Fig. 3(d).

For quantitative comparison of the deformability of RBCs, we calculate the elastic shear modulus under different osmotic conditions by fitting the linear part of Fig. 4(a) with [26]

$$D = D_0 - \frac{F}{2\pi\mu}, \quad (2)$$

where D is the diameter of RBCs in the direction perpendicular to the stretching force F , D_0 is the diameter of undeformed RBCs, and μ is the elastic shear modulus of the membrane. For our rough estimations, we assume that the cell volume remains unchanged during stretching. Under these assumptions, the elastic shear modulus

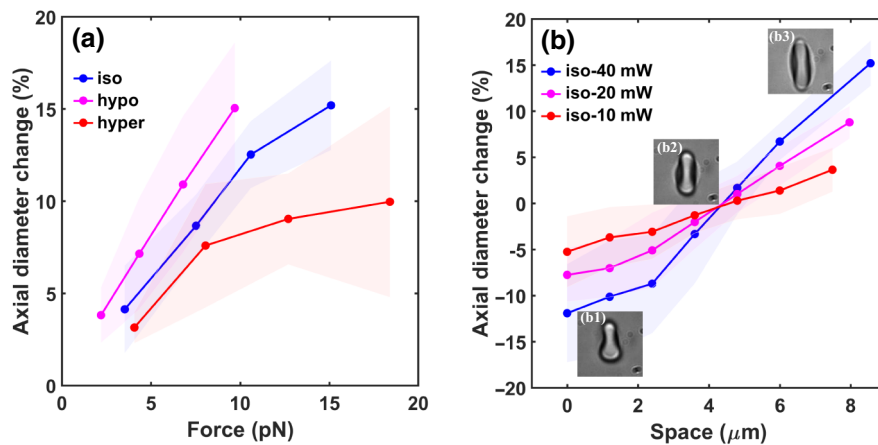


FIG. 4. Deformation of RBCs with changing forces and spacing of TOW tweezers. (a) Experimental results for human RBC manipulation under different osmotic conditions. The blue, pink, and red lines denote the experimental data recorded in isotonic, hypotonic, and hypertonic solutions, respectively. (b) Results of isotonic RBC stretching with TOW optical tweezers at different trapping powers. The blue, pink, and red lines denote the experimental data recorded at 40, 20, and 10 mW, respectively. The experimental error ranges are indicated by the shaded regions surrounding the respective curves. (b1)–(b3) Images of the deformed RBC, showing shape changes when the spacing is 0.0, 3.6, and 8.6 μm at 40 mW, respectively.

of the RBCs under different osmotic conditions are found to be $\mu \sim 1.50 \pm 0.65 \text{ pN}/\mu\text{m}$ for the hypotonic solution, $\mu \sim 1.86 \pm 0.33 \text{ pN}/\mu\text{m}$ for the isotonic solution, and $\mu \sim 3.36 \pm 0.95 \text{ pN}/\mu\text{m}$ for the hypertonic solution. These calculated results further support the notion that the RBC deformability under different osmotic conditions follows the trend hypotonic > isotonic > hypertonic. Here, notably, the magnitude of the shear modulus of RBCs differs somewhat from the reported results in the previous work because of the differences in measurement techniques and the inherent cell to cell variability [39, 49, 50]. For example, in Ref. [51], they used an indirect method (attaching beads to RBCs) to stretch RBCs and the extracted the shear modulus of RBCs was $\mu \sim 6.3 \text{ pN}/\mu\text{m}$. Moreover, as shown by the shaded region of our results in Figs. 2–4, the measurement errors of our experimental data could also come from these differences, which might partly be related to the experimental measurement duration, as the inhomogeneity of the cells could change with time during the data acquisition process when the TOW tweezers are applied to the living cells [39, 49].

We show results for squeezing and stretching isotonic RBCs as a function of spacing between two sides of the TOW beam at different laser powers in Fig. 4(b). As expected, the deformation of RBCs increases with increasing trap spacing, as well as with increasing trapping beam power. For relatively low trapping powers (10 and 20 mW), the relationship between the axial diameter change and the trap spacing is almost linear. However, when the trapping power is increased to 40 mW, such a linear relationship no longer holds. Notably, Figs. 4(b1)–4(b3) illustrate the transformation of a RBC from a squeezed state to a stretched state again. When

a RBC is squeezed, the axial diameter becomes smaller, while the diameter perpendicular to the axial direction increases slightly, as shown in Fig. 4(b1). While, thus far, most research has focused on stretching the cells, the deformability of RBCs under the action of compressive forces certainly merits further study [2–4, 6, 26–31]. With conventional optical tweezers, it is difficult to squeeze or compress a biological object, and often it requires a complicated design of a microfluidic platform with either tethering beads or counterpropagating beams. Since cell squeezing can be used to realize highly effective intracellular delivery of macromolecules [40, 41], we expect the TOW optical tweezers might play unique roles in developing photonic tools towards such applications.

IV. CONCLUSION

We perform cell manipulation (stretching and squeezing) and assessment of the deformability of RBCs under different osmotic conditions with tunable TOW optical tweezers. Our results show that the trapping force from the TOW optical tweezers is much stronger than that from normal dual-trap optical tweezers based on focused Gaussian beams. Due to the special object-adapted optical potentials [36, 37], the TOW can reduce photodamage to the cells when the same level of laser power is used as that of their Gaussian-trap counterparts. We also find that the RBCs can be squeezed when the separation of two arms of the TOW tweezers is smaller than that of the cell size. The capability of the TOW tweezers to stretch and compress cells conveniently can be implemented to study other biomechanical properties of cells and intracellular delivery of macromolecules [40, 41, 52]. In addition, for different

experimental conditions, such as the trapping laser power and background osmotic pressure, the percentage change in cell diameter and deformation dynamics are also quantitatively different. Overall, the deformability of RBCs follows the trend hypotonic > isotonic > hypertonic. Our results may be useful for the study of the biomechanical properties of living cells and cellular clusters, and the technique may be developed for distinguishing between healthy and diseased cells [53]. In particular, because of the strong trapping and pulling forces achievable at reasonably low laser power, the TOW tweezers may be employed for the real-time study of cell deformability *in vivo* [54]. Furthermore, in the role played by dual optical tweezers in microrheology measurements, the TOW tweezers could be applied to generate an oscillatory strain to realize stain-relaxation measurements [39,49], where force calibration is not required, but the tweezers are capable of discriminating between different cells. For example, based on the analysis of the temporal behavior of deformation and recovery of cells, the viscoelastic properties of fluid or cells can be obtained via a Fourier transform method used in related works [39,49,55].

ACKNOWLEDGMENTS

This work is supported by the National Key R&D Program of China (Grant No. 2017YFA0303800), the National Natural Science Foundation of China (Grants No. 11604058 and 11504184), and the Guangxi Natural Science Foundation (Grant No. 2016GXNSFBA380244).

-
- [1] N. Mohandas and P. G. Gallagher, Red cell membrane: Past, present, and future, *Blood* **112**, 3939 (2008).
- [2] Y. Kim, K. Kim, and Y. Park, in *Blood Cell—an Overview of Studies in Hematology*, edited by T. E. Moschandreas (InTech, London, 2012), pp. 167.
- [3] J. Kim, H. Lee, and S. Shin, Advances in the measurement of red blood cell deformability: A brief review, *J. Cell. Biotechnol.* **1**, 63 (2015).
- [4] D. Bento, R. Rodrigues, V. Faustino, D. Pinho, C. Fernandes, A. Pereira, V. Garcia, J. Miranda, and R. Lima, Deformation of red blood cells, air bubbles, and droplets in microfluidic devices: Flow visualizations and measurements, *Micromachines* **9**, 151 (2018).
- [5] R. Huisjes, A. Bogdanova, W. W. van Solinge, R. M. Schiffrers, L. Kaestner, and R. van Wijk, Squeezing for life – properties of red blood cell deformability, *Front. Physiol.* **9**, 656 (2018).
- [6] R. Agrawal, T. Smart, J. Nobre-Cardoso, C. Richards, R. Bhatnagar, A. Tufail, D. Shima, P. H. Jones, and C. Pavesio, Assessment of red blood cell deformability in type 2 diabetes mellitus and diabetic retinopathy by dual optical tweezers stretching technique, *Sci. Rep.* **6**, 15873 (2016).
- [7] S. Rancourt-Grenier, M.-T. Wei, J.-J. Bai, A. Chiou, P. P. Bareil, P.-L. Duval, and Y. Sheng, Dynamic deformation of red blood cell in dual-trap optical tweezers, *Opt. Express* **18**, 10462 (2010).
- [8] G. Bao and S. Suresh, Cell and molecular mechanics of biological materials.pdf, *Nat. Mater.* **2**, 715 (2003).
- [9] M. A. Meyers, P.-Y. Chen, A. Y.-M. Lin, and Y. Seki, Biological materials: Structure and mechanical properties, *Prog. Mater. Sci.* **53**, 1 (2008).
- [10] H. Zhang and K. K. Liu, Optical tweezers for single cells, *J. R. Soc. Interface* **5**, 671 (2008).
- [11] A. C. De Luca, G. Rusciano, R. Ciancia, V. Martinelli, G. Pesce, B. Rotoli, L. Selvaggi, and A. Sasso, Spectroscopical and mechanical characterization of normal and thalassemic red blood cells by Raman tweezers, *Opt. Express* **16**, 7943 (2008).
- [12] G. B. Liao, Y. Q. Chen, P. B. Bareil, Y. Sheng, A. Chiou, and M. S. Chang, Radiation pressure on a biconcave human Red Blood Cell and the resulting deformation in a pair of parallel optical traps, *J. Biophotonics* **7**, 782 (2014).
- [13] J. Guck, R. Ananthakrishnan, H. Mahmood, T. J. Moon, C. C. Cunningham, and J. Käs, The optical stretcher: A novel laser tool to micromanipulate cells, *Biophys. J.* **81**, 767 (2001).
- [14] X. Chen, G. Xiao, X. Han, W. Xiong, H. Luo, and B. Yao, Observation of spin and orbital rotation of red blood cell in dual-beam fibre-optic trap with transverse offset, *J. Opt.* **19**, 055612 (2017).
- [15] X. Liu, J. Huang, Y. Li, Y. Zhang, and B. Li, Rotation and deformation of human red blood cells with light from tapered fiber probes, *Nanophotonics* **6**, 309 (2017).
- [16] M. Gu, S. Kuriakose, and X. Gan, A single beam near-field laser trap for optical stretching, folding and rotation of erythrocytes, *Opt. Express* **15**, 1369 (2007).
- [17] R. Sroka, E. Spyratou, L. D. Lilge, M. Makropoulou, and A. A. Serafetinides, Red blood cell micromanipulation with elliptical laser beam profile optical tweezers in different osmolarity conditions, *SPIE* **8092**, 80920T (2011).
- [18] A. Kauppila, M. Kinnunen, A. Karmenyan, and R. Myllyl, Measurement of the trapping efficiency of an elliptical optical trap with rigid and elastic objects, *Appl. Opt.* **51**, 5705 (2012).
- [19] K. B. Roth, K. B. Neeves, J. Squier, and D. W. Marr, Imaging of a linear diode bar for an optical cell stretcher, *Biomed. Opt. Express* **6**, 807 (2015).
- [20] S. K. Mohanty, A. Uppal, and P. K. Gupta, Optofluidic stretching of RBCs using single optical tweezers, *J. Biophotonics* **1**, 522 (2008).
- [21] C. Zensen, I. E. Fernandez, O. Eickelberg, J. Feldmann, and T. Lohmuller, Detecting swelling states of red blood cells by “cell-fluid coupling spectroscopy”, *Adv. Sci.* **4**, 1600238 (2017).
- [22] D. C. Silva, C. N. Jovino, C. A. Silva, H. P. Fernandes, M. Milton Filho, S. C. Lucena, A. M. D. Costa, C. L. Cesar, M. L. Barjas-Castro, B. S. Santos, and A. Fontes, Optical tweezers as a new biomedical tool to measure zeta potential of stored red blood cells, *PloS one* **7**, e31778 (2012).
- [23] M. M. Haque, M. G. Moisescu, S. Valkai, A. Der, and T. Savopol, Stretching of red blood cells using an electro-optics trap, *Biomed. Opt. Express* **6**, 118 (2015).
- [24] M. Xie, A. Shakoob, and C. Wu, Manipulation of biological cells using a robot-aided optical tweezers system, *Micromachines* **9**, 245 (2018).

- [25] M. A. de Oliveira, D. S. Moura, A. Fontes, and R. E. de Araujo, Damage induced in red blood cells by infrared optical trapping: An evaluation based on elasticity measurements, *J. Biomed. Opt.* **21**, 75012 (2016).
- [26] S. Henon, G. Lenormand, A. Richert, and F. Gallet, A new determination of the shear modulus of the human erythrocyte membrane using optical tweezers, *Biophys. J.* **76**, 1145 (1999).
- [27] M. Dao, C. T. Lim, and S. Suresh, Mechanics of the human red blood cell deformed by optical tweezers, *J. Mech. Phys. Solids* **51**, 2259 (2003).
- [28] C. T. Lim, M. Dao, S. Suresh, C. H. Sow, and K. T. Chew, Large deformation of living cells using laser traps, *Acta Mater.* **52**, 1837 (2004).
- [29] Y. Tan, D. Sun, J. Wang, and W. Huang, Mechanical characterization of human red blood cells under different osmotic conditions by robotic manipulation with optical tweezers, *IEEE Trans. Biomed. Eng.* **57**, 1816 (2010).
- [30] H. Song, Y. Liu, B. Zhang, K. Tian, P. Zhu, H. Lu, and Q. Tang, Study of *in vitro* RBCs membrane elasticity with AOD scanning optical tweezers, *Biomed. Opt. Express* **8**, 384 (2017).
- [31] J. E. Mancuso and W. D. Ristenpart, Stretching of red blood cells at high strain rates, *Phys. Rev. Fluids* **2**, 101101 (2017).
- [32] T. Betz, M. Lenz, J. F. Joanny, and C. Sykes, ATP-dependent mechanics of red blood cells, *Proc. Natl. Acad. Sci. U. S. A.* **106**, 15320 (2009).
- [33] F. Schlosser, F. Rehfeldt, and C. F. Schmidt, Force fluctuations in three-dimensional suspended fibroblasts, *Philos. Trans. R. Soc., B* **370**, 20140028 (2015).
- [34] H. Turlier, D. A. Fedosov, B. Audoly, T. Auth, N. S. Gov, C. Sykes, J. F. Joanny, G. Gompper, and T. Betz, Equilibrium physics breakdown reveals the active nature of red blood cell flickering, *Nat. Phys.* **12**, 513 (2016).
- [35] J. Mills, L. Qie, M. Dao, C. Lim, and S. Suresh, Nonlinear elastic and viscoelastic deformation of the human red blood cell with optical tweezers, MCB-TECH SCIENCE PRESS **1**, 169 (2004).
- [36] A. S. Bezryadina, D. C. Preece, J. C. Chen, and Z. Chen, Optical disassembly of cellular clusters by tunable “tug-of-war” tweezers, *Light Sci. Appl.* **5**, e16158 (2016).
- [37] J. Lamstein, A. Bezryadina, D. Preece, J. C. Chen, and Z. Chen, Optical tug-of-war tweezers: Shaping light for dynamic control of bacterial cells (invited paper), *Chin. Opt. Lett.* **15**, 030010 (2017).
- [38] See the Supplemental Material at <http://link.aps.org/supplemental/10.1103/PhysRevApplied.12.064060> for videos of Figs. 1(b), 2(b–d), and 3(a–c); a video of an RBC trapped and rotated stably and reliably in a given observation plane, and captions for the eight videos.
- [39] A.-I. Bunea and J. Glückstad, Strategies for optical trapping in biological samples: Aiming at microrobotic surgeons, *Laser Photonics Rev.* **0**, 1800227 (2019).
- [40] A. Sharei *et al.*, A vector-free microfluidic platform for intracellular delivery, *Proc. Natl. Acad. Sci. U. S. A.* **110**, 2082 (2013).
- [41] A. Kollmannsperger, A. Sharei, A. Raulf, M. Heilemann, R. Langer, K. F. Jensen, R. Wieneke, and R. Tampé, Live-cell protein labelling with nanometre precision by cell squeezing, *Nat. Commun.* **7**, 10372 (2016).
- [42] R. Gautam, Y. Xiang, J. Lamstein, Y. Liang, A. Bezryadina, G. Liang, T. Hansson, B. Wetzel, D. Preece, A. White, M. Silverman, S. Kazarian, J. Xu, R. Morandotti, and Z. Chen, Optical force-induced nonlinearity and self-guiding of light in human red blood cell suspensions, *Light: Sci. Appl.* **8**, 31 (2019).
- [43] M. Diez-Silva, M. Dao, J. Han, C.-T. Lim, and S. Suresh, Shape and biomechanical characteristics of human red blood cells in health and disease, *MRS Bull.* **35**, 382 (2010).
- [44] H. W. G. Lim, M. Wortis, and R. Mukhopadhyay, Stomatocyte-discocyte-echinocyte sequence of the human red blood cell: Evidence for the bilayer-couple hypothesis from membrane mechanics, *Proc. Natl. Acad. Sci. U. S. A.* **99**, 16766 (2002).
- [45] M. P. Miccio L, F. Merola, P. A. Netti, and P. Ferraro, Red blood cell as an adaptive optofluidic microlens.pdf, *Nat. Commun.* **6**, 6502 (2015).
- [46] P. Jones, O. Maragò, and G. Volpe, *Optical Tweezers: Principles and Applications* (Cambridge University Press, Cambridge, 2015).
- [47] E. Loth, Drag of non-spherical solid particles of regular and irregular shape, *Powder Technol.* **182**, 342 (2008).
- [48] M. Friebe, J. Helfmann, and M. C. Meinke, Influence of osmolarity on the optical properties of human erythrocytes, *J. Biomed. Opt.* **15**, 055005 (2010).
- [49] M. Tassieri, Linear microrheology with optical tweezers of living cells “is not an option”!, *Soft Matter* **11**, 5792 (2015).
- [50] Y. A. Ayala, Bruno Pontes, Diney S. Ether, Luis B. Pires, Glauber R Araujo, Susana Frases, L. F. Romão, M. Farina, V. Moura-Neto, N. B. Viana, and H. M. Nussenzveig, Rheological properties of cells measured by optical tweezers, *BMC Biophys.* **9**, 5 (2016).
- [51] D. A. Fedosov, B. Caswell, and G. E. Karniadakis, A multiscale red blood cell model with accurate mechanics, rheology, and dynamics, *Biophys. J.* **98**, 2215 (2010).
- [52] B. S. Ahluwalia, P. McCourt, A. Oteiza, J. S. Wilkinson, T. R. Huser, and O. G. Hjeltnes, Squeezing red blood cells on an optical waveguide to monitor cell deformability during blood storage, *Analyst* **140**, 223 (2015).
- [53] J. S. T. Gongora and A. Fratallocchi, Optical force on diseased blood cells: Towards the optical sorting of biological matter, *Opt. Lasers Eng.* **76**, 40 (2016).
- [54] M. C. Zhong, X. B. Wei, J. H. Zhou, Z. Q. Wang, and Y. M. Li, Trapping red blood cells in living animals using optical tweezers, *Nat. Commun.* **4**, 1768 (2013).
- [55] M. Tassieri, J. Ramírez, N. C. Karayiannis, S. K. Sukumaran, and Y. Masubuchi, i-Rheo GT: Transforming from time to frequency domain without artifacts, *Macromolecules* **51**, 5055 (2018).